Chapter 5

Sea State Models

5.1 Summary

(i) Two types of sea surface temperature analysis systems are operated at JMA. One is a high resolution analysis using satellite remote sensing data and *in-situ* observation data to provide real-time ocean information. The other is an analysis based on *in-situ* observation data to monitor long-term variations in the ocean such as El Niño events and global warming.

(ii) A global ocean data assimilation system (MOVE/MRI.COM-G) has been operated at JMA since 2008 for the monitoring of El Niño and the Southern Oscillation (ENSO). MOVE/MRI.COM-G consists of an ocean general circulation model (MRI.COM) and an objective analysis scheme. The output of MOVE/MRI.COM-G, along with the atmospheric analysis, is given to a coupled ocean-atmosphere model for ENSO prediction and seasonal forecast of climate in Japan.

(iii) Another ocean data assimilation system for the Western North Pacific (MOVE/MRI.COM-WNP) has been operated since 2008, aiming to analyze and predict variations of sea-water temperature, salinity and current associated with eddy-scale oceanic phenomena, such as the Kuroshio, Oyashio and mid-scale eddies in the seas adjacent to Japan.

(iv) JMA operates three wave models: the Global Wave Model (GWM), the Coastal Wave Model (CWM), and the Shallow-water Wave Model (SWM). The GWM and CWM, for the seas around Japan, are based on the MRI-III, which is developed in the Meteorological Research Institute (MRI) of JMA. The SWM, which is applied to several bays and seas near shore, is based on the WAM, which is a well known wave model and used in many organizations.

(v) JMA has operated storm surge models. One model is for Japan region and predicts storm surges generated by tropical and extra-tropical cyclones. The model runs eight times a day and provides 33or 30 hours forecasts for 385 points along Japanese coastlines. The other is for Asian region, which is developed in the framework of the Storm Surge Watch Scheme of WMO. The model runs four times a day and predicts up to 72 hours forecast, and horizontal storm surge map and time series at selected points are issued to the members of Typhoon Committee.

(vi) A numerical sea ice model has been operated at JMA to support sea ice forecast for the southern part of the Sea of Okhotsk. The model forecasts distributions and concentrations of sea ice for one week based on dynamic and thermodynamic equations in the winter season.

(vii) An oil spill prediction model has been ready for operation at JMA since 1999. The model is an advection-diffusion model to predict distributions of spilled oil. The operation is triggered when a large-scale oil spill occurs in the offshore seas. Effects of transport by sea surface winds, ocean waves and sea surface currents, turbulent diffusion, evaporation and emulsification are considered in the model.

5.2 Sea Surface Temperature Analysis

5.2.1 Merged Satellite and *In-situ* Data Global Daily Sea Surface Temperature

High-resolution daily sea surface temperatures (SSTs) in the global ocean on a grid of $0.25° \times 0.25°$ are objectively analyzed for ocean information services and for providing boundary conditions of the atmospheric short and medium range prediction models and the North Pacific Ocean models (see Section 3.2, Section 3.5 and Section 5.5; Kurihara *et al.* (2006)). SSTs obtained from the infrared radiometer of AVHRRs on the NOAA and MeTop polar orbiting meteorological satellites are used together with *in-situ* SST observations. While a major portion of the *in-situ* data are obtained through the Global Telecommunication System, still many are obtained from domestic organizations via facsimile, e-mail and postal mail.

Satellite-derived SST anomalies (SSTA) from daily SST climatologies are decomposed into two temporal-scale and three spatial-scale components: long and short timescales with a cutoff period of 53 days, and large, middle and small scales with cutoff wavelengths of 580km and 143km. The middle scale is aimed to represent the SST signals caused by eddy-scale phenomena. The small scale is aimed to represent meso-scale signals. The signals varying with a period shorter than 27 days are cut off, because the noise of the data in this range is considerably large. The long timescale signals represent the intra-seasonal variation, and the short timescale signals represent variation influenced by atmospheric condition, such as a tropical cyclone reducing SSTs.

The large-scale and long-timescale components of SSTAs from AVHRR are calibrated with *in-situ* SSTAs using Poisson's equation (Reynolds (1987)). The space-time optimum interpolation (OI) is applied to each component. Zero value is adopted as the first guess. The space-time correlation coefficients and the RMS values of the first guess error and the satellites' observation errors were statistically estimated a priori from the satellites' data themselves, using the method of Kuragano and Kamachi (2000). Daily SST is a sum of the components of interpolated SSTAs and the daily climatologies (Figure 5.2.1).

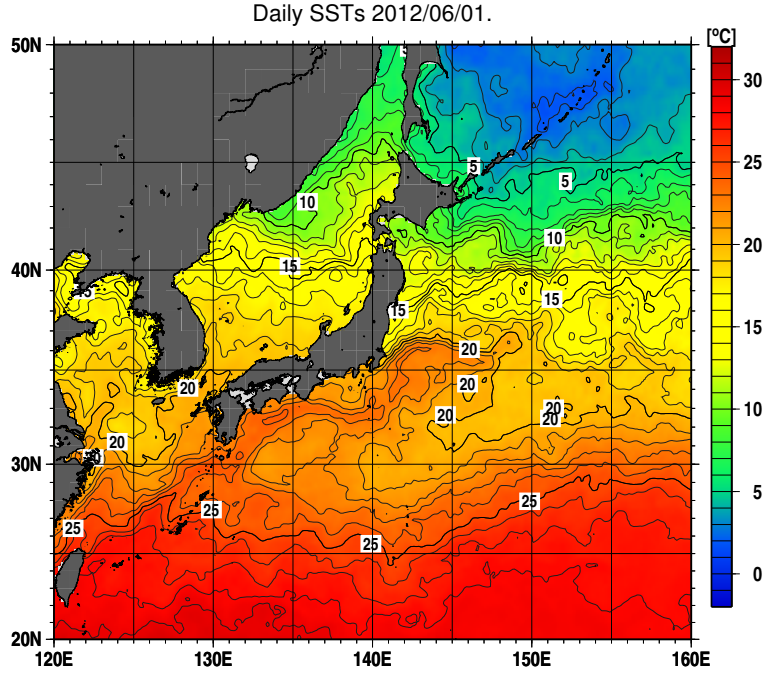

Figure 5.2.1: An example of analyzed SSTs

5.2.2 Daily Sea Surface Analysis for Climate Monitoring and Predictions

The Sea Surface Temperature (SST) analysis for climate monitoring at JMA is based on the method described in Ishii *et al.* (2005), which is summarized in the following.

The SST analysis has a resolution of 1° latitude and 1° longitude. The east-west grid points start at 0.5°E and end at 0.5°W. The north-south grid points start at 89.5°S, and end at 89.5°N. The analysis uses optimum interpolation method. The deviation of the previous day's analysis from normal is multiplied by 0.95 and is used as a first guess. The analysis is performed daily and uses the marine meteorological data for 7 days centered at the day of interest. The observed data in a day are averaged in $1.5^\circ \times 1.5^\circ$ box before analyzing data by optimum interpolation method to save the processing time of analysis.

The bias corrections for the past SST observation reports were performed by the way of Folland and Parker (1995). The quality control of observed data is performed by checking ship tracks, dates and positions of reports, and then erroneous data are automatically corrected in compiling marine meteorological data in JMA. Moreover, with observed data deviations from climatological values during the three months including the day of interest, biases of the data having the same ship call signs are estimated, and call signs having large biased data are listed automatically in a blacklist through the daily analysis. The daily analysis (final analysis) is performed with delay of 31 days from real time to allow delayed observations to be used sufficiently. Additionally as quick look analyses for the real time utilization, the analyses for the 30-day period following the final analysis are done every day.

The information of sea ice concentration is made use of in estimating SSTs in the polar oceans.

The daily updated operational SST data are utilized as follows with historical ones.

1. Monitoring of equatorial Pacific SSTs, El Niño/ La Niña evolutions and global warming over 100 years.
2. Input of the operational Ocean Data Assimilation System (MOVE/MRI.COM-G) and historical oceanic analysis (see Section 5.3).
3. Input of the JMA Climate Data Assimilation System (JCDAS) and Japanese 25-year Re-analysis (see Section 2.10).
4. Input of Ensemble Prediction Systems for one-month forecasts (see Section 3.3).

The monthly averaged SST data are made available through the Tokyo Climate Center web site[1] and characteristics of the data are described in Japan Meteorological Agency (2006) which is available in the Web page of Tokyo Climate Center[2].

5.3 Ocean Data Assimilation System

Following successful development of a ocean data assimilation system (MOVE/MRI.COM) by the Meteorological Research Institute (MRI) of JMA, JMA has been operating two types of the MOVE/MRI.COM since 2008. One is the global system (MOVE-G) for the monitoring of El Niño and the Southern Oscillation (ENSO), which replaced JMA-ODAS described in the previous report. The other is the Western North Pacific system (MOVE-WNP) for analyzing eddy-scale oceanic phenomena in the seas adjacent to Japan, which is a successor of COMPASS-K described in the previous report. In the following subsections, firstly a brief outline of the MOVE/MRI.COM is provided. Secondly, some examples of the MOVE-G and MOVE-WNP are presented.

5.3.1 Ocean General Circulation Model and Objective Analysis Scheme

The MOVE/MRI.COM consists of an ocean general circulation model (MRI.COM) and an objective analysis scheme (MOVE). The details of MOVE/MRI.COM are described in Usui et al. (2006).

MRI.COM (Ishikawa *et al.* 2005) is a multilevel model that solves primitive equations under the hydrostatic and the Boussinesq approximation. The σ-z vertical coordinate is adopted with which the layer thickness

[1] http://ds.data.jma.go.jp/tcc/tcc/products/elnino/cobesst/cobe-sst.html
[2] http://ds.data.jma.go.jp/tcc/tcc/library/MRCS_SV12/index_e.htm

near the surface follows the surface topography to allow the freely elevating surface (Hasumi 2006). For the nonlinear momentum advection, the generalized enstrophy-preserving scheme (Arakawa 1972) and the scheme that contains the concept of diagonally upward/downward mass momentum fluxes along the sloping bottom are applied. The vertical viscosity and diffusivity are determined by the turbulent closure scheme of Noh and Kim (1999). In MOVE-G, isopycnal mixing (Gent and McWilliams 1990) is used for horizontal turbulent mixing, and harmonic viscosity with the parameterization of Smagorinsky (1963) is used for momentum. In MOVE-WNP, on the other hand, a biharmonic operator is used for horizontal turbulent mixing, and a biharmonic friction with a Smagorinsky-like viscosity (Griffies and Hallberg 2000) is used for momentum. The values of wind stress, heat and fresh water fluxes to drive the model are produced with the routinely operated JMA Climate Data Assimilation System (JCDAS; see Section 2.10), which is almost the same system as the Japanese 25-year Re-Analysis (JRA25; Onogi *et al.* 2007).

The analysis scheme adopted in MOVE is a multivariate three-dimensional variational (3DVAR) analysis scheme with vertical coupled Temperature-Salinity (T-S) Empirical Orthogonal Function (EOF) modal decomposition (Fujii and Kamachi 2003). Amplitudes of the T-S EOF modes above 1500 m are employed as control variables and the optimal temperature and salinity fields are represented by the linear combination of the EOF modes. In this system, the model domain is divided into several subregions and vertical T-S EOF modes are calculated from the observed T-S profiles for each subregion. The 3DVAR results are inserted into the model temperature and salinity fields above 1500 m by the incremental analysis updates (Bloom *et al.* 1996).

These in-situ observations are reported from ships, profiling floats and moored or drifting buoys through the GTS and other communication systems. In MOVE/MRI.COM, not only in-situ observations of subsurface temperature and salinity, but also satellite altimeter data are assimilated into the model. The results of sea surface temperature analysis, which are analyzed independently from the MOVE/MRI.COM, are also assimilated as observational data; the COBE-SST (see Subsection 5.2.2) grid-point values are used for MOVE-G, and the MGDSST (see Subsection 5.2.1) grid-point values are used for MOVE-WNP.

5.3.2 Ocean Data Assimilation System for Global ocean (MOVE-G)

The horizontal resolution is 1.0° latitude and 1.0° longitude except for the 15°S-15°N band, where the latitudinal grid spacing decreases to the minimum of 0.3° between 6°S and 6°N (see Figure 5.3.1). The model has 50 vertical levels, 24 of which are placed above 200 meters (see Figure 5.3.2). The model has realistic bottom topography, and the maximum depth of the bottom is set to 5000 meters. The computational domain is global, excluding the higher latitudes than 75°S and 75°N. With regard to sea ice, daily climatological data are applied to MRI.COM. Additionally, the deviation of the model sea surface temperature (SST) from the daily analyzed SST for climate (COBE-SST; Ishii *et al.* 2005) is referred to in calculating long-wave radiation to keep the model SST closer to the observation.

The latest assimilation results are obtained once in five days, and the targeted term is 3-7 days before the assimilation is carried out. The assimilation data for the same term are updated every five days using additional delayed-mode observation data until the term reaches 39-43 days before the final assimilation.

The output from MOVE-G is used in various forms for the monitoring of ENSO at JMA, and some products for the equatorial Pacific region are distributed in a couple of publications, namely, "Monthly Highlights on Climate System" and "El Niño Outlook". Figure 5.3.3 is one of such charts of the MOVE-G, which shows the depth-longitude sections of temperature and its anomalies. The charts in the reports are also made available through the Tokyo Climate Center Web page[3].

5.3.3 Ocean Data Assimilation System for the Western North Pacific (MOVE-WNP)

The model domain spans from 117°E to 160°W zonally and from 15°N to 65°N meridionally. The horizontal resolution is variable: it is 1/10° from 117°E to 160°E and 1/6° from 160°E to 160°W, and 1/10° from 15°N to 50°N and 1/6° from 50°N to 65°N. There are 54 levels in the vertical direction with thickness increasing 1 m at the surface to 600 m near the bottom (see Figure 5.3.4). Oceanic states at the side boundaries are replaced by those from a North Pacific model with a horizontal resolution of 1/2° (one-way nesting). A sea ice model

[3] http://ds.data.jma.go.jp/tcc/tcc/index.html

with the thermodynamics of Mellor and Kantha (1989) and the elastic-viscous-plastic rheology of Hunke and Dukowicz (1997) is also applied.

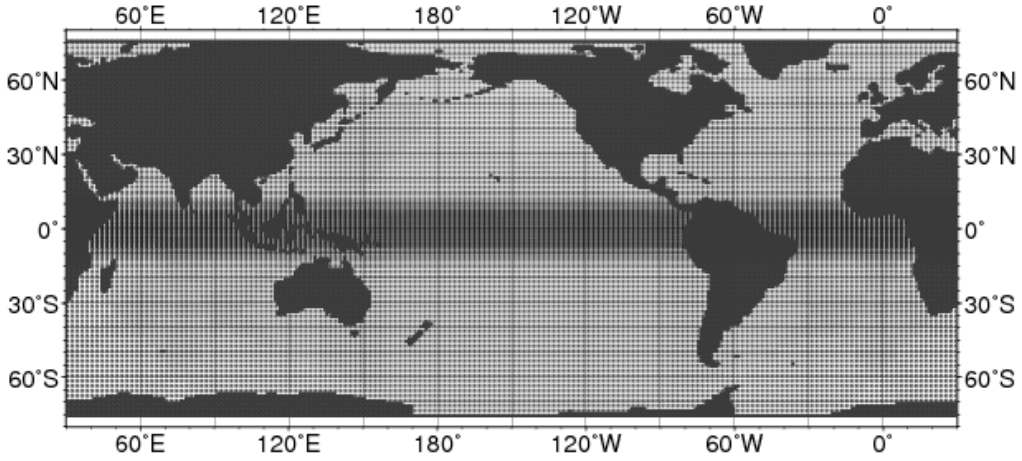

Figure 5.3.1: The MOVE-G horizontal grids

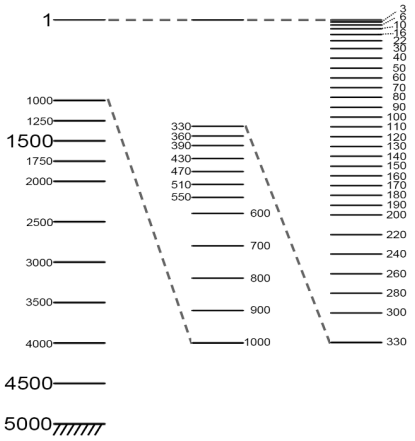

Figure 5.3.2: The MOVE-G vertical levels which indicate depths in meter

Figure 5.3.5 shows the predicted ocean current fields at a depth of 50m, which was calculated by the forecast run from the initial condition of 1 May 2012. The assimilated fields are also shown in the figure. The figure shows that the undulation of the Kuroshio path was successfully predicted in the forecast run. The assimilation run is implemented every five days. The output from MOVE-WNP is used as initial condition of the ocean forecasting model with one month prediction period. The results of the operational assimilation, nowcast and forecast runs are provided on JMA's web site and those of assimilation and nowcast runs are available on the NEAR-GOOS RRTDB[4].

[4] http://goos.kishou.go.jp/

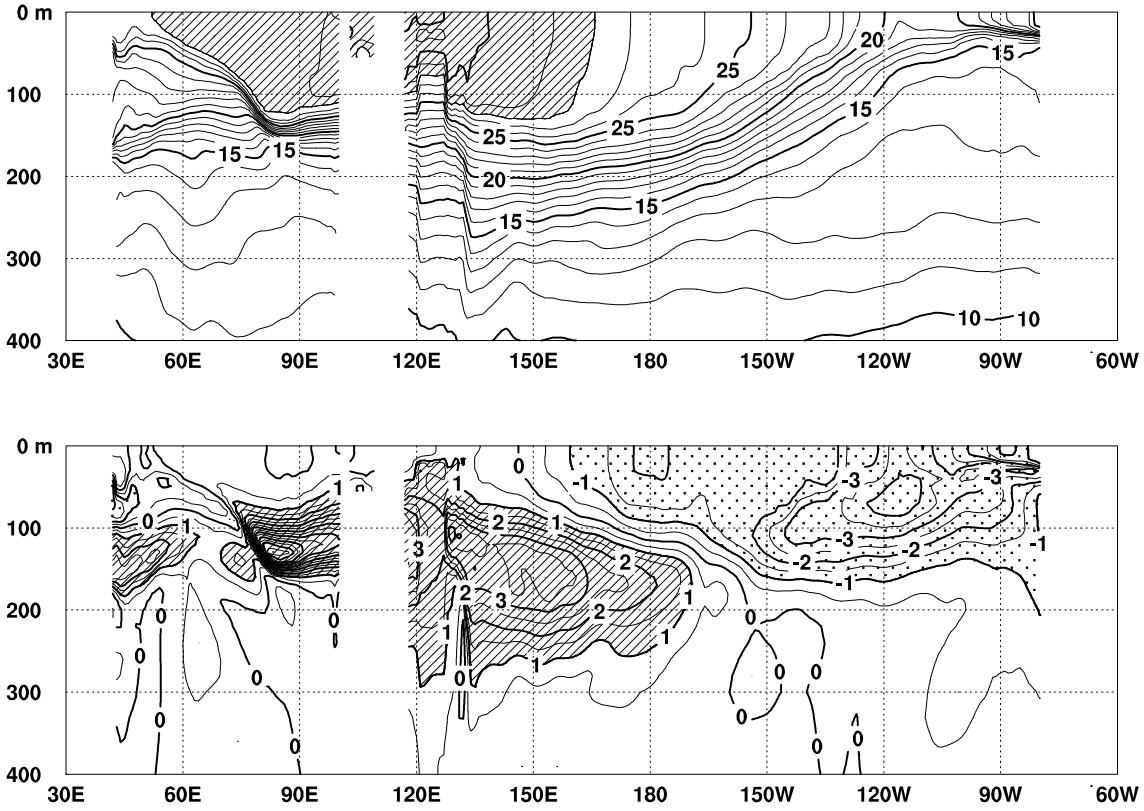

Figure 5.3.3: Depth-longitude cross sections of monthly mean temperature and temperature anomalies along the equator in the Indian and Pacific Ocean for November 2010 by MOVE-G. Base period for normal is 1981-2010.

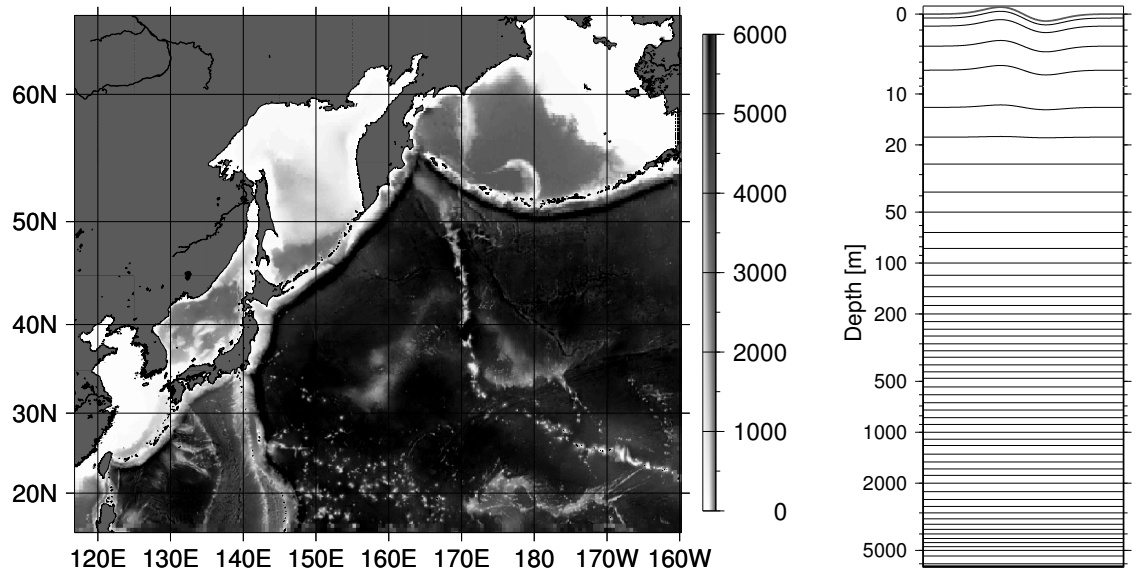

Figure 5.3.4: Bottom topography (left panel) and vertical levels (right panel) of OGCM for the Western North Pacific.

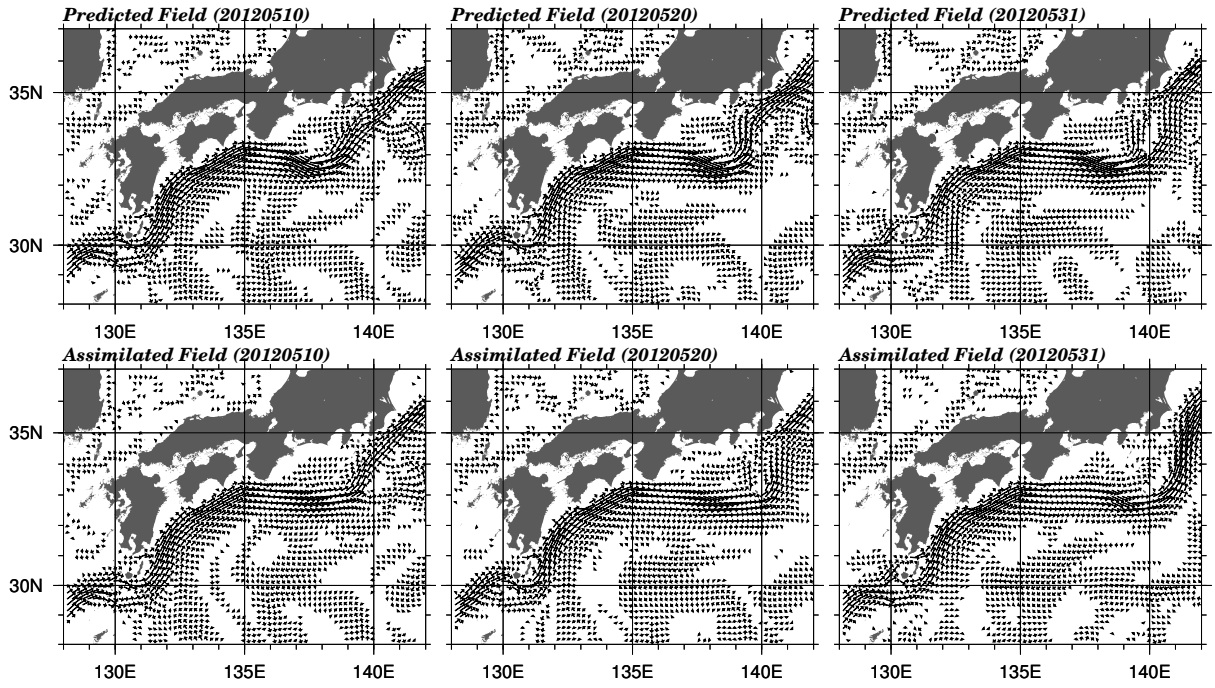

Figure 5.3.5: Horizontal current fields around 50m depth. Upper panels show the results of prediction using the initial condition of 1 May 2012. Lower panels are depicted using assimilation results.

5.3.4 Future plan

The Meteorological Research Institute (MRI) of JMA is now in process of developing a new ocean data assimilation system which is composed of a new version of MRI.COM (Tsujino *et al.* 2010) and the improved MOVE system. The new model will cover the global ocean including the Arctic Ocean, and its resolution will be higher than the present model. Introduction of an active sea-ice model is under consideration.

While the MOVE-WNP is aimed at monitoring sub meso-scale features such as a variation of the Kuroshio path, demands for information on smaller scale phenomena (e.g. the Kuroshio frontal waves) are increasing. JMA/MRI is now developing a new ocean model, which has higher horizontal resolution and schemes considering tidal effect.

5.4 Ocean Wave Models

5.4.1 Introduction

The Japan Meteorological Agency (JMA) operates three wave models: the Global Wave Model (GWM), the Coastal Wave Model (CWM) and the Shallow-water Wave Model (SWM), all of which are classified as the third-generation wave model.

The GWM and the CWM are based on the MRI-III, which was originally developed in the Meteorological Research Institute of JMA. The current versions of the GWM and the CWM, which only consider deep water waves, have been in operations since May 2007. The specifications of the GWM and the CWM are given in Table 5.4.1 and the model domains are shown in Figure 5.4.1.

The SWM is based on the WAM (The WAMDI Group 1988), but was modified at the National Institute for Land and Infrastructure Management of the Ministry of Land, Infrastructure, Transport, and Tourism (MLIT) and was put into operation under a cooperative framework with MLIT's Water and Disaster Management Bureau. The specifications of the SWM are given in Table 5.4.2. The SWM has high resolution of 1 minute,

Table 5.4.1: Specifications of the Global Wave Model and the Coastal Wave Model.

Model name	Global Wave Model	Coastal Wave Model
Type of wave model	spectral model (third-generation wave model, MRI-III)	
Area	global 75°N – 75°S 180°W – 0° – 180°E	coastal sea of Japan 50°N – 20°N 120°E – 150°E
Grid size	0.5° × 0.5° (720 × 301)	0.05° × 0.05° (601 × 601)
Time step (advection term) (source term)	 10 minutes 30 minutes	 1 minutes 3 minutes
Calculated time (from 00UTC, 06UTC, 18UTC) (from 12UTC)	 84 hours 264 hours	 84 hours 84 hours
Spectral component	900 components 25 frequencies from 0.0375 to 0.3 Hz (logarithmically partitioned) 36 directions	
Initial condition	hindcast	
Boundary condition		Global Wave Model
Wind field	Global Spectral Model (GSM)	
	Fujita's empirical formula and a corresponding gradient wind for a typhoon	

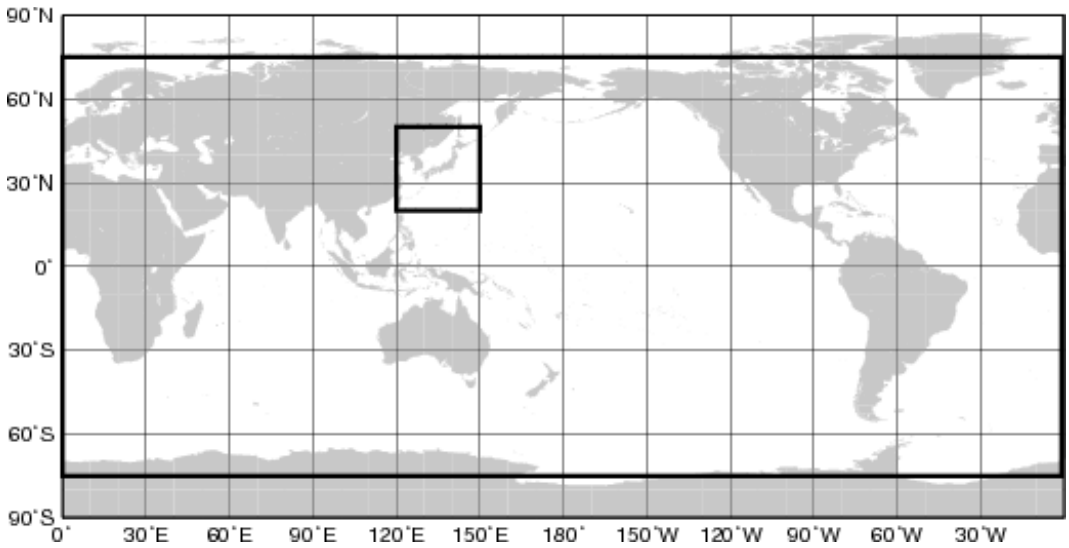

Figure 5.4.1: The calculation area of the Global Wave Model (outer thick line) and the Coastal Wave Model (inner thick line).

Table 5.4.2: Specifications of the Shallow-water Wave Model.

Type of wave model	spectral model (third-generation wave model, WAM)		
Areas	Domain name	Grid size	Integration domain
	Off Tomakomai	121 × 43	42.70°N – 42.00°N 141.00°E – 0° – 143.00°E
	Sendai Bay	37 × 43	38.45°N – 37.75°N 140.90°E – 0° – 141.50°E
	Tokyo Bay	37 × 43	35.75°N – 35.05°N 139.55°E – 0° – 140.15°E
	Ise Bay	61 × 43	35.05°N – 34.35°N 136.45°E – 0° – 137.45°E
	Harima-Nada Osaka Bay	79 × 49	34.85°N – 34.05°N 134.15°E – 0° – 135.45°E
	Suo-Nada Iyo-Nada Aki-Nada	109 × 67	34.40°N – 33.30°N 131.00°E – 0° – 132.80°E
	Ariake Sea	43 × 49	33.25°N – 32.45°N 130.05°E – 0° – 130.75°E
	Off Niigata	55 × 37	38.40°N – 37.80°N 138.35°E – 0° – 139.25°E
Grid resolution	1′ × 1′		
Time step (advection term) (source term)	 1 minutes 1 minutes		
Calculated time	33hours		
Spectral component	1260 components 35 frequencies from 0.0418 to 1.1 Hz (logarithmically partitioned) 36 directions		
Initial condition	hindcast		
Boundary condition	Coastal Wave Model		
Wind field	Meso-Scale Model (MSM)		
	Fujita's empirical formula and a corresponding gradient wind for a typhoon		

including shallow water effects. However, the SWM is applied to only limited areas, as shown in Figure 5.4.2. The products of the SWM are only used within JMA and MLIT's Regional Development Bureaus.

5.4.2 Structure of the Ocean Wave Models

All of the wave models are spectral model which is usually used in operational forecasts. The physical element is wave energy density (spectrum) of each frequency and direction, namely two-dimensional (directional) wave spectrum. The basic equation is the energy balance equation

$$\frac{\partial F}{\partial t} + \nabla(C_g \cdot F) = S_{net} = S_{in} + S_{nl} + S_{ds} + S_{btm} \tag{5.4.1}$$

where $F(f, \theta, x, t)$ is the two dimensional spectrum dependent on the frequency f and the wave direction θ, $C_g(f, \theta, x)$ is the group velocity, which becomes simply $C_g(f)$ for deep water waves. S_{net} is the net source function which consists of four terms: S_{in}, S_{nl}, S_{ds}, and S_{btm}. The four terms are briefly explained as follows. The model numerics of the MRI-III are described since those of the WAM has many references (Janssen 2004).

1. S_{in}: the energy input from wind. The S_{in} is generally expressed as the form $S_{in} = A + BF$, where A shows linear wave growth and BF exponential growth. In the MRI-III, the formula of Cavaleri and Rizzoli (1981) is used for linear growth

$$A = 1.5 \times 10^{-3} \left(u_*^4 / 2\pi g^2\right) \exp[-(f_{PM}/f)^4] \, (\max(0, \cos(\theta - \theta_W))^4 \tag{5.4.2}$$

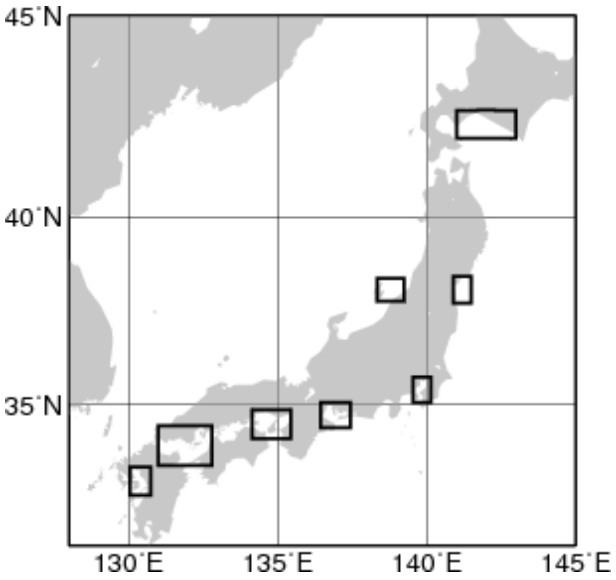

Figure 5.4.2: The calculation area of the Shallow-water Wave Model.

where θ is a direction of wave spectrum, u_* the friction velocity of wind, θ_W the wind direction, g the gravitational acceleration. In general, this term has little influence on wave growth except very early stage. On the other hand, the exponential term BF has a key role in wave growth. In the MRI-III, The B is expressed as

$$B(f, u_*, \theta_W - \theta) = c_{in}\left(\frac{u_*}{C_p}\right)^2 \cos^3(\theta_W - \theta)/|\cos(\theta_W - \theta)|. \tag{5.4.3}$$

where C_p is the phase speed of deep water waves, namely $C_p = \dfrac{g}{\omega} = \dfrac{g}{2\pi f}$.

This expression is based on Mitsuyasu and Honda (1982) and Plant (1982).

2. S_{nl}: the nonlinear energy transfer by resonant interaction. Because the rigorous calculation requires much computation time, a practical scheme, the Discrete Interaction Approximation (DIA) (Hasselmann *et al.* 1985), was developed. This scheme uses only one parameter for the set of four resonant waves and is widely used in many third-generation wave models.

$$\left.\begin{array}{l} f_1 = f_2 = f, \\ f_3 = f(1+\lambda) = f_+, \\ f_4 = f(1-\lambda) = f_-, \\ \theta_1 = \theta_2 = \theta, \\ \theta_3 - \theta = \pm\cos^{-1}\left\{\left(1 + 2\lambda + 2\lambda^3\right)/(1+\lambda)^2\right\}, \\ \theta_4 - \theta = \mp\cos^{-1}\left\{\left(1 - 2\lambda - 2\lambda^3\right)/(1-\lambda)^2\right\}. \end{array}\right\} \tag{5.4.4}$$

$$\left\{\begin{array}{c} \delta S_{nl} \\ \delta S^+_{nl} \\ \delta S^-_{nl} \end{array}\right\} = \left\{\begin{array}{c} -2(\Delta f \Delta\theta)/(\Delta f \Delta\theta) \\ (1+\lambda)(\Delta f \Delta\theta)/(\Delta f_+ \Delta\theta) \\ (1-\lambda)(\Delta f \Delta\theta)/(\Delta f_- \Delta\theta) \end{array}\right\}$$

$$\times C f^{11} g^{-4}\left[F^2\left\{\frac{F_+}{(1+\lambda)^4} + \frac{F_-}{(1-\lambda)^4}\right\} - 2\frac{F F_+ F_-}{(1-\lambda^2)^4}\right] \tag{5.4.5}$$

where $F \equiv F(f,\theta)$, $F_+ \equiv F(f_+,\theta_3)$, $F_- \equiv F(f_-,\theta_4)$. The coefficient C is determined to be fitted to the exact calculation. Hasselmann *et al.* (1985) defined the parameters as $\lambda = 0.25$ which corresponds to $\theta_3 - \theta = \pm 11.5°$, $\theta_4 - \theta = \mp 33.6°$, and $C = 3 \times 10^7$. It is turned out that the DIA calculation gives much accurate estimation by multiplying the parameters. In the MRI-III, S_{nl} is calculated by DIA scheme but with three configurations. The used parameters are $\lambda_1 = 0.19 (C_1 = 1.191 \times 10^7)$, $\lambda_2 = 0.23 (C_2 = 6.835 \times 10^6)$, and $\lambda_3 = 0.33 (C_3 = 1.632 \times 10^6)$.

3. S_{ds}: the energy dissipation due to wave breaking and so on. In the MRI-III, dissipation terms are expressed as local energy dissipation proposed by Ueno (1998).

$$S_{ds} = -c_b \frac{u_*}{g^3} f^7 \left(F(f,\theta)\right)^2 \tag{5.4.6}$$

where c_b is a coefficient and determined to fit with wave generation. In the MRI-III, swell decay process which is slightly artificial is also included.

$$S_{sds} = -2.96 \times 10^{-6} \tanh\left[4 \left(f_s - f\right) / f_p\right] F(f,\theta), \tag{5.4.7}$$

Where $f_p = 0.156 g / U_{10N}$ stands for the peak frequency of the Pierson-Moskowitz (PM) spectrum from the 10m height wind speed U_{10N}. This decay function is applied to the spectrum whose frequency is smaller than $f_s = 1.8 f_p$ and only when significant wave height is larger than 1.5m.

4. S_{btm}: the energy loss by bottom friction. This term is not yet included in the MRI-III which deal with only deep water.

5.4.3 Wind Field

Wind fields for the GWM and the CWM are given by the Global Spectral Model (GSM), while the SWM uses Meso-Scale Model (MSM) winds. In all the models, wind fields around typhoons were modified with an empirical method. Typhoons are one of major sources to produce extremely high waves in the western North Pacific, and accurate wave forecasts are crucial to prevent shipwreck and coastal disasters. Since the NWP models sometimes do not predict correct typhoon conditions such as intensity or location, wind fields by operationally analyzed / forecasted typhoon are implanted onto the NWP winds (what we call "bogus wind") , when a typhoon exists in the western North Pacific. Moreover, the change of a typhoon course may drastically change the wave field especially in small region of the SWM. Therefore, wave fields are also predicted in five cases when typhoon is assumed to move the successive path of five points (center, faster, slower, right end and left end) on the typhoon forecast error circle.

The bogus winds are made as the following way. Sea level pressure distribution near a typhoon is assumed to have a profile of Fujita's empirical formula (Fujita 1952)

$$P(r) = P_\infty - \frac{P_\infty - P_0}{\sqrt{1 + (r/r_0)^2}} \tag{5.4.8}$$

where P_∞, P_0 and r_0 denote the ambient pressure, the central pressure of the typhoon, and the scaling factor of the radial distribution of the pressure, respectively. Surface winds near the typhoon are estimated from the pressure field by assuming the gradient wind balance with modifications based on the typhoon movement and surface friction effects.

5.4.4 Initial Condition

The initial conditions for the wave models are given by the 6-hour forecast of the previous initial run. Wind fields for the initial conditions are given by the GSM and the MSM initiated 6 hours before. An assimilation scheme (Kohno *et al.* 2011) for the GWM and the CWM has just been introduced in October 2012. In this system, initial conditions (wave spectra) are modified based on the significant wave heights by the Objective Wave Analysis System (Kohno *et al.* 2009), which automatically analyzes wave heights with observations by

radar altimeters of satellites, buoys, coastal wave recorders and ships. This change will improve the prediction of ocean wave field, especially in shorter forecast time.

5.4.5 Examples of Wave Prediction

Figure 5.4.3 is an example of the 24-hour prediction of wave fields by GWM. The chart contains contours of significant wave heights and mean wave direction at selected grid points.

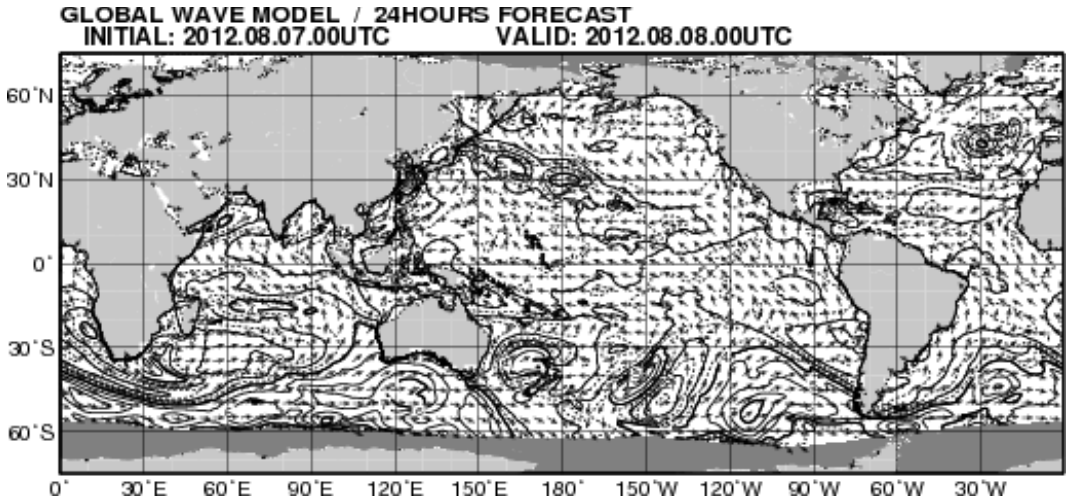

Figure 5.4.3: An example of 24-hour prediction of ocean wave by the Global Wave Model with the initial time of 00UTC 7 August 2012. Significant wave heights are contoured with dashed lines for half a meter, solid lines for every meter and thick solid lines for every 4 meters. Wave directions are represented by arrows for selected grid points. Area of sea ice is dark-shaded.

Figure 5.4.4 is a chart of the 24-hour prediction of wave fields by CWM.

5.4.6 Improvement and Development

The new assimilation scheme has just been introduced and is needed to be improved, as well as the MRI-III model numerics improvements.

The target area of the SWM is going to be added in due course. Furthermore, new version of MRI-III, including shallow water effects, has been developed to be used as the SWM.

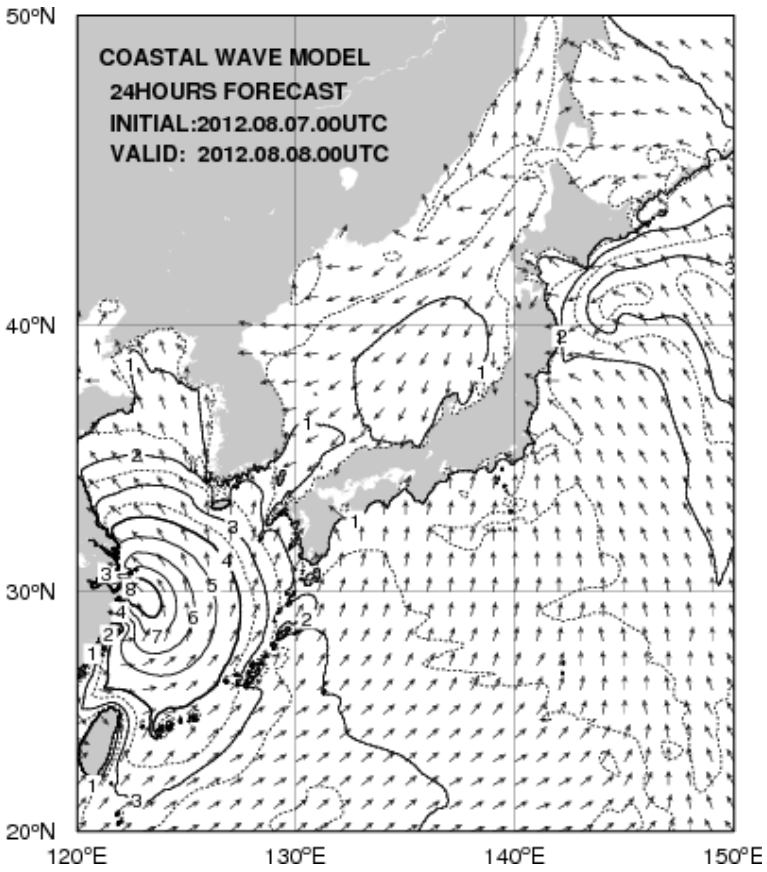

Figure 5.4.4: An example of 24-hour prediction around Japan by the Coastal Wave Model with the initial time of 00UTC 7 August 2012. Notations are the same as in Figure 5.4.3. The high wave was predicted around a tropical cyclone in the East China.

5.5 Storm Surge Model

5.5.1 Japan Area Storm Surge Model

5.5.1.1 Introduction

Since Japan has suffered from many storm surge disasters over the years, accurate and timely forecasts and warnings are critical to mitigating the threat to life and property from such storm surges.

Japan Meteorological Agency (JMA), which is responsible for issuing storm surge warnings, has operated a numerical storm surge model since 1998 to provide basic information for the warnings.

Numerical storm surge prediction started in July 1998 only when a typhoon exists. The storm surge model has been modified in enlarging the model domain, prediction for the extratropical cyclone case, extending of forecast time and adding advection terms, etc. Since May 2010, for more detailed information and warnings, a new storm surge model with higher resolution (approximately 1 km mesh) and the gridded astronomical tide analysis method have been operated.

5.5.1.2 Dynamics

Storm surges are mainly caused by the effect of wind setup due to strong onshore winds on sea surface and inverse barometer effect associated with pressure drop in a low pressure system. The effect of wind setup is proportional to the square of wind speed and inversely proportional to water depth, and related with the coastal topography, that is, it is amplified in a bay opened against the wind.

The storm surge model operated in the JMA is almost the same as the one described in Higaki *et al.* (2009). This model includes the ocean model and the part which makes the meteorological fields that drive the ocean model. To predict the temporal and spatial variations of sea level in response to such meteorological disturbances, the storm surge model utilizes two-dimensional shallow water equations. The shallow water equations consist of vertically integrated momentum equations in two horizontal directions:

$$\frac{\partial U}{\partial t} + u\frac{\partial U}{\partial x} + v\frac{\partial U}{\partial y} - fV = -g(D+\eta)\frac{\partial(\eta-\eta_0)}{\partial x} + \frac{\tau_{\mathrm{sx}}}{\rho_w} - \frac{\tau_{\mathrm{bx}}}{\rho_w} \tag{5.5.1a}$$

$$\frac{\partial V}{\partial t} + u\frac{\partial V}{\partial x} + v\frac{\partial V}{\partial y} + fU = -g(D+\eta)\frac{\partial(\eta-\eta_0)}{\partial y} + \frac{\tau_{\mathrm{sy}}}{\rho_w} - \frac{\tau_{\mathrm{by}}}{\rho_w} \tag{5.5.1b}$$

and the continuity equation:

$$\frac{\partial \eta}{\partial t} + \frac{\partial U}{\partial x} + \frac{\partial V}{\partial y} = 0 \tag{5.5.2}$$

where U and V are volume fluxes in the x- and y-directions, defined as:

$$U \equiv \int_{-D}^{\eta} u\,dz \tag{5.5.3a}$$

$$V \equiv \int_{-D}^{\eta} v\,dz \tag{5.5.3b}$$

f is the Coriolis parameter; g is the gravity acceleration; D is the water depth below mean sea level; η is the surface elevation; η_0 is the inverse barometer effect converted into the equivalent water column height; ρ_w is the density of water; τ_{sx} and τ_{sy} are x- and y-components of wind stress on sea surface; and τ_{bx} and τ_{by} are stresses of bottom friction, respectively.

The equations are solved by numerical integration using an explicit finite difference method. Regarding grid system, the staggered (or Arakawa-C) grid (Arakawa and Lamb 1977) is adopted.

5.5.1.3 Meteorological Forcing

The fields of surface wind and atmospheric pressure predicted by the Meso-Scale Model (MSM) are required as external forcing for the storm surge model. When a tropical cyclone (TC) exists around Japan, a simple parametric TC model is also used.

The simple parametric TC model (or referred to as bogus) is introduced in order to take into account the error of TC track forecast and its influence on storm surge forecasting. To consider the influence of TC track uncertainty on the occurrence of storm surge, we conduct five runs of the storm surge model with five possible TC tracks. These TC tracks are prescribed at the center and at four points on the forecast circle within which a TC is forecasted to exist with a probability of 70% (Figure 5.5.1):

1. Center track
2. Fastest track
3. Rightward biased track
4. Slowest track
5. Leftward biased track

and used to make meteorological fields with the parametric TC model.

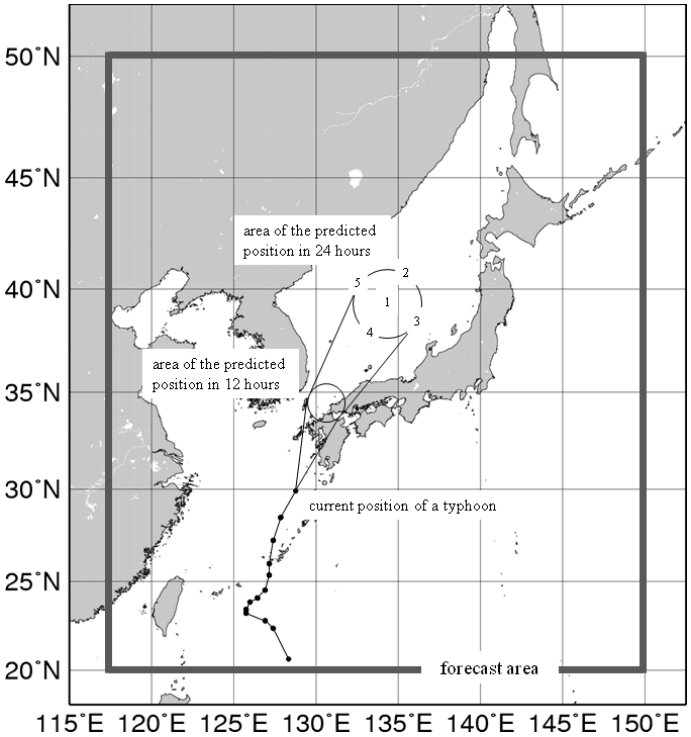

Figure 5.5.1: TC tracks of bogus and the domain of the Japan area storm surge model

The simple parametric TC model utilizes the Fujita's formula (Fujita 1952) that represents the radial pressure distribution in a TC:

$$P = P_\infty - \frac{P_\infty - P_c}{\sqrt{1 + (r/r_0)^2}} \tag{5.5.4}$$

and the gradient wind relation:

$$-\frac{v_g^2}{r} - f v_g = -\frac{1}{\rho}\frac{\partial P}{\partial r} \tag{5.5.5}$$

In Eq. (5.5.4), P is an atmospheric pressure at distance r from the center of a TC, P_∞ is the atmospheric pressure at an infinitely distant point, P_c is the pressure at TC center and r_0 is the scaling factor of the radial distribution of the pressure. In Eq. (5.5.5), ρ is the density of air, v_g is the gradient wind.
To represent the asymmetry of wind field **w** in a TC, the moving velocity vector of the TC multiplied by a weight that decays exponentially with the distance from TC center is added to the gradient wind:

$$\mathbf{w} = C_1 \left\{ \mathbf{v_g} + \mathbf{C} \cdot \exp\left(-\pi \frac{r}{r_e}\right) \right\} \tag{5.5.6}$$

C is the the moving velocity vector of the TC, r_e is the coefficient of decay.

Analysis and forecast information on TC, such as center position, central pressure and maximum wind are applied to these formulas to synthesize the wind and pressure fields (Konishi 1995).

5.5.1.4 Specifications of the Model

Table 5.5.1 gives the specifications of the storm surge model. The finest horizontal resolution of the model is $45''$(lon) $\times$ $30''$(lat) (approximately 1km mesh). The model domain covers the entire Japan.

Table 5.5.1: Specifications of the Japan area storm surge model

Model	2-dimensional model
Grid	Lat-Lon Arakawa-C grid
Region	20°N - 50°N, 117.5°E - 150°E
Resolution	approximately 1, 2, 4, 8, 16 km (Adaptive mesh)
Time step	4 seconds
Initial time	00, 03, 06, 09, 12, 15, 18, 21 (UTC)
Forecast time	00, 06, 12, 18 (UTC): 30 hours 03, 09, 15, 21 (UTC): 33 hours
Member	TC case: 6 members (MSM+5 bogus) no TC case: 1 member (MSM)

Since the storm surge is the shallow water long wave, its phase speed is proportional to the square root of water depth. It is inefficient to set all grids with the same resolution from a viewpoint of computer resources. Therefore, the adaptive mesh refinement (Berger and Oliger 1984) in which the mesh is fine over the shallow water and coarse over the deep water is adopted. The resolution is varied for 5 levels (1, 2, 4, 8 and 16 km) with the water depth (Figure 5.5.2). This method makes the storm surge calculations more efficient than the normal lat-lon grid system.

The storm surge model runs 8 times a day (every 3 hours) and calculates storm surge predictions up to 30 or 33 hours ahead. Initial values are generated by a previous calculation using the newest MSM prediction as the forcing (hindcast). Since the initial values are not so important as the one in atmospheric models, assimilation of observation data is not conducted.

The model computes only storm surges, i.e. anomalies from the level of astronomical tides. However, storm tides (storm surge plus astronomical tide) are also needed in issuing a storm surge warning. Astronomical tides are predicted by using harmonic analyses of sea level observations. The JMA developed the gridded astronomical tide method which calculates the astronomical tide even on the no-observation grid (Subsection 5.5.3). After the computation of the storm surge model, the level of astronomical tide for the coastal area is added to the predicted storm surge.

Then the results are sent to Local Meteorological Observatories that issue storm surge warnings to their responsible areas.

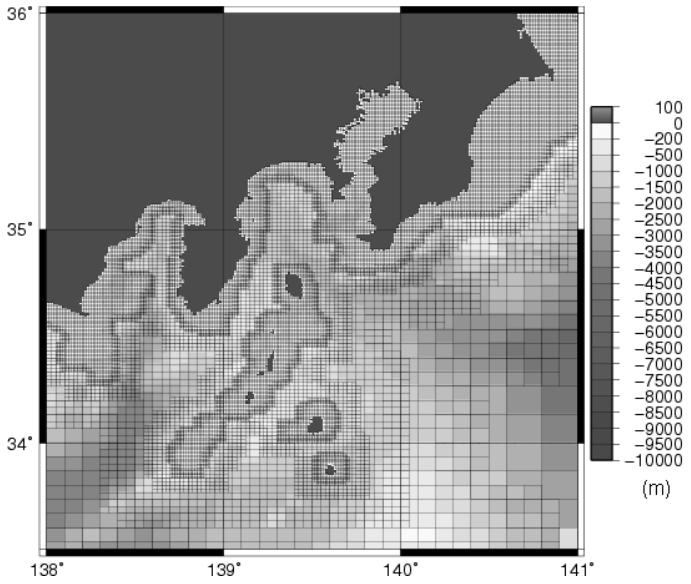

Figure 5.5.2: Horizontal grid system and water depth of the storm surge model (around Kanto region)

5.5.1.5 Verification

Accuracy of the storm surge prediction depends on accuracy of the storm surge model itself and atmospheric model. We investigated the accuracy of the storm surge model itself using the storm surge predictions driven by the atmospheric analysis data.

Figure 5.5.3 shows a scatter diagram of the predicted storm surges against the observed values. The statistical period is from 2004 to 2008. Observation from 120 tide stations, which are managed by the JMA, the Japan Coast Guard and the Geographical Survey Institute, are used. The figure shows that most errors of storm surge predictions lie in the range of ± 50 cm. It is supposed that the large errors mainly result from the factors which are not included in the storm surge model, i.e., the effect of wave setup, ocean currents and sea water stratification, etc.

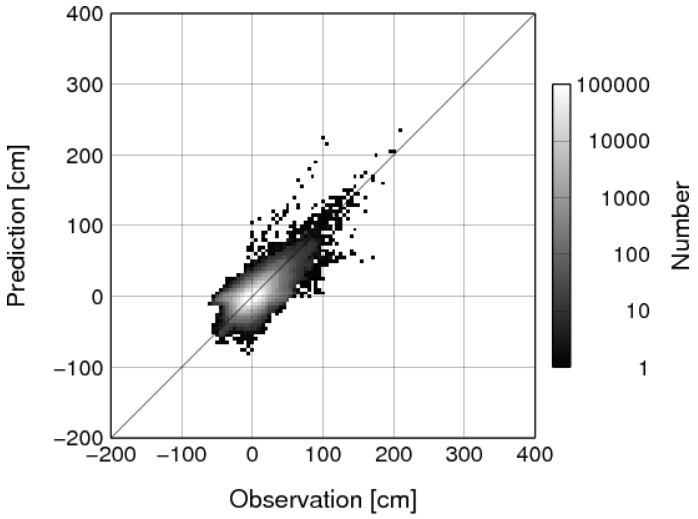

Figure 5.5.3: Scatter diagram of predicted storm surges against observed values

Figure 5.5.4 shows the best track of typhoon MELOR (T0918). The typhoon MELOR passed the eastern part of Japan and caused storm surge disasters especially in Mikawa bay on 8 October 2009. Figure 5.5.5 (a) shows the distributions of storm surge around Mikawa bay. The model well predicted the extreme storm surges by the wind setup in closed-off section of Mikawa bay. Figure 5.5.5 (b) shows the time series of storm surge at the port of Mikawa. Though the peak surge was slightly underestimated, the time of peak surge was exactly predicted.

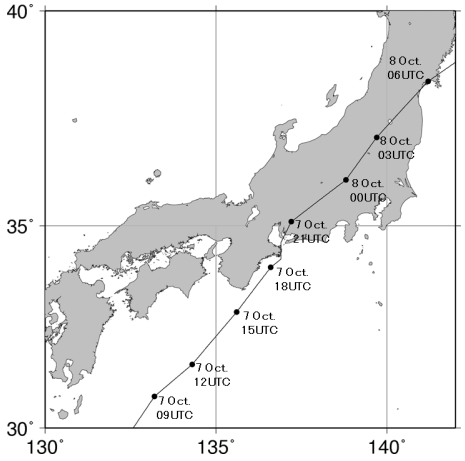

Figure 5.5.4: The best track of typhoon MELOR (T0918)

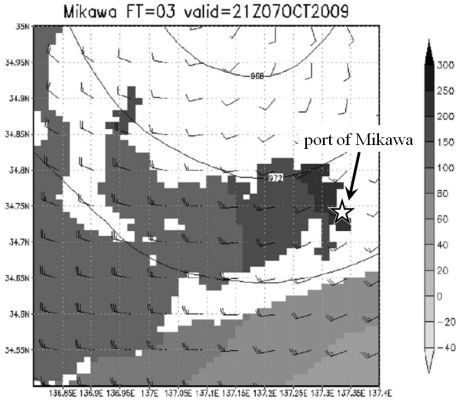

(a) Distribution of storm surge at 21UTC 8 October around Mikawa bay predicted by the storm surge model

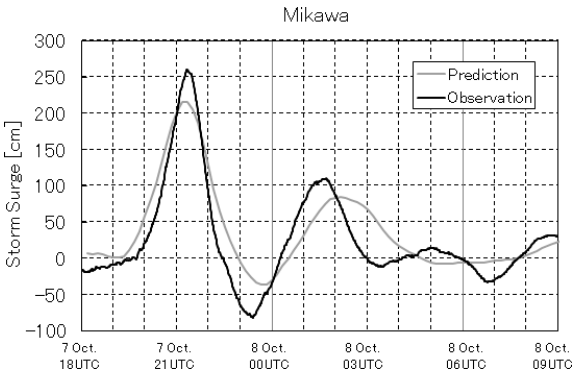

(b) Time series of storm surge at the port of Mikawa

Figure 5.5.5: Distribution of storm surge and timeseries at the port of Mikawa

5.5.2 Asia Area Storm Surge Model

5.5.2.1 Introduction

In recent years, heavy storm surge disasters occurred worldwide, such as the one in the coast of the Gulf of Mexico caused by Hurricane Katrina in 2005, the one in the coast of Bangladesh by Cyclone Sidr in 2007, and the one in the coast of Myanmar by Cyclone Nargis in 2008. By these storm surges more than thousands of people suffered. The countermeasures for storm surges and inundation are crucial.

In response to a request by the WMO Executive Council (60th session, June 2008), WMO initiated the development of a regional Storm Surge Watch Scheme (SSWS) in regions affected by tropical cyclones. In relation to the western North Pacific and the South China Sea, the ESCAP/WMO Typhoon Committee (41st session, January 2009) endorsed a commitment by the RSMC Tokyo - Typhoon Center to prepare storm surge forecasts with the aim of strengthening the storm surge warning capabilities of National Meteorological and Hydrological Services (NMHSs) in the region. JMA began development of a storm surge model for the Asia region in 2010, in collaboration with Typhoon Committee Members who provide sea level observation and sea bathymetry data. Horizontal distribution maps of predicted storm surges and time series charts have been published on JMA's Numerical Typhoon Prediction website (Hasegawa *et al.* 2012).

5.5.2.2 Dynamics

The basic equations of the Asia area storm surge model are nearly the same as those of the Japan area storm surge model (Subsection 5.5.1) except that advection terms are omitted. The equations of the model incorporate vertically integrated momentum fluxes under the influence of the earth's rotation with gravity acceleration:

$$\frac{\partial U}{\partial t} - fV = -g(D+\eta)\frac{\partial(\eta-\eta_0)}{\partial x} + \frac{\tau_{\mathrm{sx}}}{\rho_w} - \frac{\tau_{\mathrm{bx}}}{\rho_w} \tag{5.5.7a}$$

$$\frac{\partial V}{\partial t} + fU = -g(D+\eta)\frac{\partial(\eta-\eta_0)}{\partial y} + \frac{\tau_{\mathrm{sy}}}{\rho_w} - \frac{\tau_{\mathrm{by}}}{\rho_w} \tag{5.5.7b}$$

and the continuity equation:

$$\frac{\partial \eta}{\partial t} + \frac{\partial U}{\partial x} + \frac{\partial V}{\partial y} = 0 \tag{5.5.8}$$

Definitions of each variables and constants are the same as those of the Japan area storm surge model. The wind stresses are expressed as:

$$\tau_{\mathrm{sx}} = c_d \rho_a W u_w \tag{5.5.9a}$$

$$\tau_{\mathrm{sy}} = c_d \rho_a W v_w \tag{5.5.9b}$$

where c_d is the drag coefficient, ρ_a is the density of air, $W \equiv \sqrt{u_w^2 + v_w^2}$ is the wind speed, and (u_w, v_w) is the wind velocity. The drag coefficient is set from the results of Smith and Banke (1975) and Frank (1984):

$$c_d = \begin{cases} (0.63 + 0.066W) \times 10^{-3} & (W < 25 m/s) \\ \{2.28 + 0.033(W-25)\} \times 10^{-3} & (W \geq 25 m/s) \end{cases} \tag{5.5.10}$$

5.5.2.3 Data

The bathymetry data for the storm surge model is mainly made from the 2-minute Global Gridded Elevation Data (ETOPO2) of NGDC/NOAA (Figure 5.5.6). The bathymetry data was partly modified with local bathymetry data provided by the Typhoon Committee Members, which enable more accurate forecast.

The astronomical tides are determined by harmonic analysis using the past tide observation data provided by the Typhoon Committee members.

5.5.2.4 Meteorological Forcing

In the operation of the Asia area storm surge model, two kinds of meteorological forcing field are used. One is a simple parametric TC model, and the other is the products of the JMA operational Global Spectral Model (GSM). The simple parametric TC model of the Asia area storm surge model is the same one as of the Japan area storm surge model (Subsection 5.5.1).

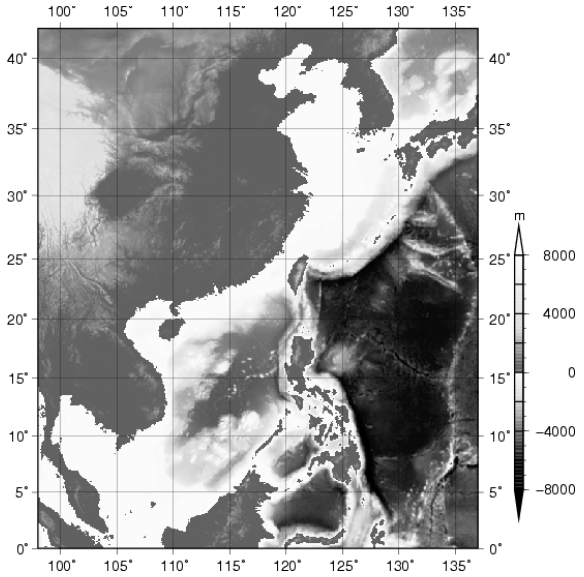

Figure 5.5.6: Model domain and topography of the Asia area storm surge model

5.5.2.5 Specifications of the Model

Table 5.5.2 shows the outline of the specifications of the Asia area storm surge model. The horizontal grid resolution is 2 minutes, corresponding to a distance of about 3.7 km. The model covers almost all areas in the RSMC Tokyo - Typhoon Center area of responsibility (Figure 5.5.6). It runs four times a day (every 6 hours), and calculates storm surge predictions up to 72 hours ahead. Each calculation takes about 10 minutes, and storm surge distribution maps are created using the results. When no typhoon is expected nor exist during the forecast time, the model calculates the hindcast only for the next run, and no distribution maps are produced.

The 3-hourly distribution maps of the whole domain and enlarged versions showing only the areas around typhoon are available up to 72 hours. The time series charts include predicted/astronomical tide, storm surge, sea level pressure and surface wind.

Table 5.5.2: Specifications of the Asia area storm surge model

Model	2-dimensional linear model
Grid	Lat-Lon Arakawa-C grid
Region	0° - 42°N, 98°E - 137°E
Resolution	2-minutes mesh (approximately 3.7 km mesh)
Time step	8 seconds
Initial time	00, 06, 12, 18 (UTC)
Forecast time	72 hours
Member	1 member

5.5.2.6 Verification

To examine the performance of the Asia area storm surge model, we verified the model accuracy by comparing predicted values with observed ones. In this verification, hourly storm surge predictions were compared with observations at seven tide stations. The predictions are calculated by the GSM analysis data (Sep. 2007 to Dec. 2010) and the parametric TC model with typhoon best track data made by RSMC Tokyo - Typhoon Center.

Figure 5.5.7 shows a scatter diagram of the predicted storm surges against the observed values. The predicted values include all those for 1-hour through 72-hour forecast time. The figures show that the surge predictions lie in the range of 100 cm.

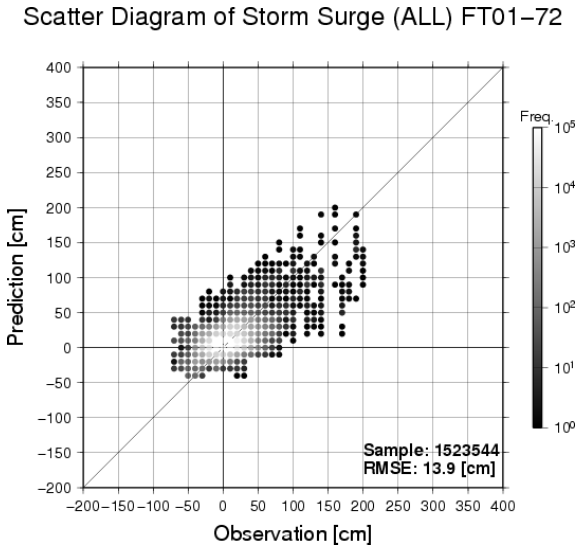

Figure 5.5.7: Scatter diagram of predicted storm surges against observed values

Figure 5.5.8 shows a storm surge distribution map for Typhoon KOPPU (T0915), which generated extremely high storm surges in Hong Kong and Macao and made landfall on the coast of southern China, and a time series chart at Macao. The extremely high storm surges are well represented by the Asia area storm surge model.

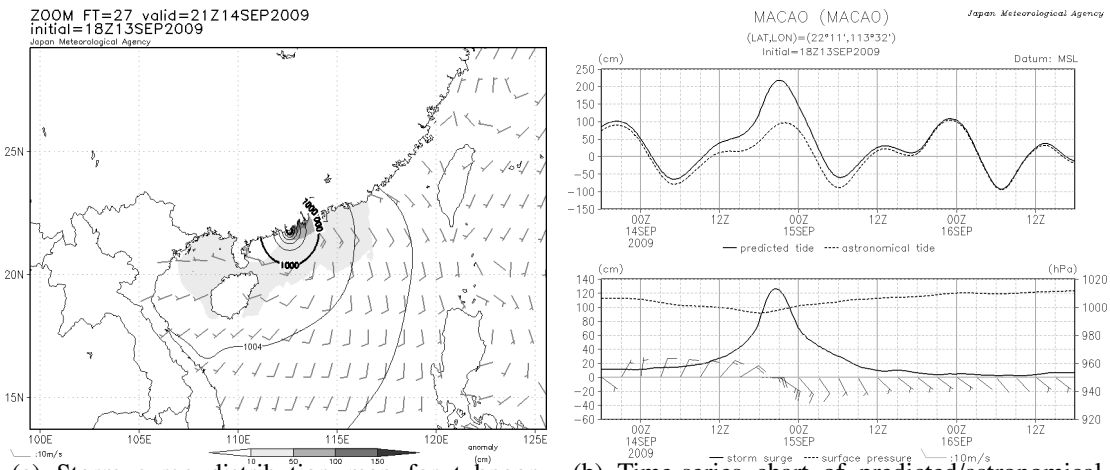

(a) Storm surge distribution map for tyhpoon KOPPU (T0915)

(b) Time-series chart of predicted/astronomical tides and storm surge at Macao

Figure 5.5.8: Distribution of storm surge and timeseries at Macao

5.5.3 Astronomical Tide Analysis

5.5.3.1 Introduction

The model explained in Subsection 5.5.1 only calculates storm surges, in other words, anomalies from the level of the astronomical tides. But, prediction of storm tides, which are storm surges plus the astronomical tides, are needed for issuing storm surge warnings. Since 2010, JMA issues storm surge warnings for all coastal areas in Japan. Therefore the analyses of astronomical tides at any Japanese coast are required. JMA developed a new analysis method of astronomical tides for the coastal seas around Japan.

5.5.3.2 Analysis Method

The variation of tides is expressed as a composition of periodic oscillations in various frequencies such as semi-diurnal, diurnal and annual tides. Semi-diurnal and diurnal tides are caused by gravitational forces of the moon and the sun. Annual tides are brought by seasonal variation of seawater temperature and sea surface pressure. Harmonic constants which are the sets of amplitudes and phases for each tidal constituent are derived by harmonic analysis. As for tide station, they are derived by analyzing hourly tidal observation data. But, it is impossible to gain the harmonic constants at arbitrary coastal points by using this method.

In order to analyze astronomical tides at any point, we calculate the first guess and assimilate the harmonic constants at tide stations. The procedures of analysis for short-period tides (semi-diurnal and diurnal tides) and long-period tides (annual tides) are described below. The schematic diagram is shown in Figure 5.5.9. Constituents used in this method are shown on Table 5.5.3.

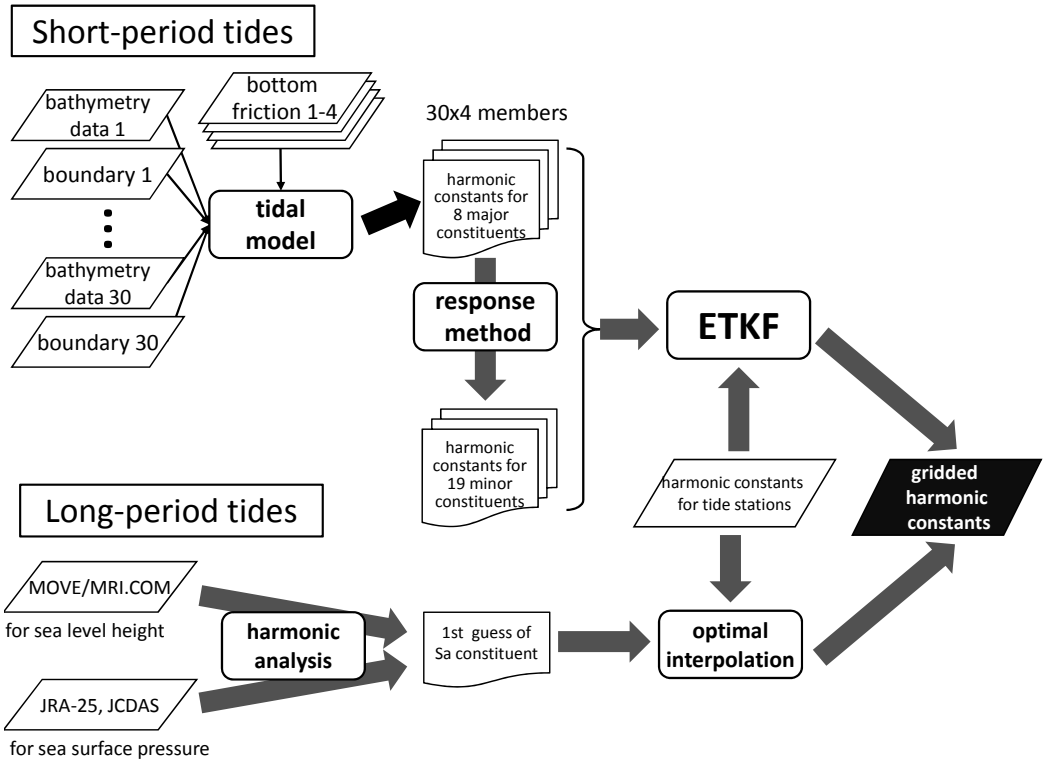

Figure 5.5.9: Schematic flow chart of astronomical tide analysis

Table 5.5.3: List of constituents used in astronomical tide analysis. "Major" and "minor" mean constituents estimated by a tidal model, and those estimated by the response method using major constituents, respectively.

Name	Type	Major/Minor	Name	Type	Major/Minor
S_a	annual	-	θ_1	diurnal	minor
$2Q_1$	diurnal	minor	J_1	diurnal	minor
σ_1	diurnal	minor	OO_1	diurnal	minor
Q_1	diurnal	major	$2N_2$	semi-diurnal	minor
ρ_1	diurnal	minor	μ_2	semi-diurnal	minor
O_1	diurnal	major	N_2	semi-diurnal	major
MP_1	diurnal	minor	ν_2	semi-diurnal	minor
M_1	diurnal	minor	M_2	semi-diurnal	major
χ_1	diurnal	minor	λ_2	semi-diurnal	minor
π_1	diurnal	minor	L_2	semi-diurnal	minor
P_1	diurnal	major	T_2	semi-diurnal	minor
K_1	diurnal	major	S_2	semi-diurnal	major
ψ_1	diurnal	minor	R_2	semi-diurnal	minor
ϕ_1	diurnal	minor	K_2	semi-diurnal	major

5.5.3.3 Short-period Tides

Constituents which amplitude is relatively large (major 8 constituents) are estimated using a tidal model of Oregon State University Tidal Inversion Software (OTIS) package (Egbert and Erofeeva 2002). OTIS consists of three components: the data preparation, the ocean dynamics and the data assimilation. We only use the linearized version of the ocean dynamics (tidal model) in which Fourier transform is applied to eliminate time variable:

$$i\omega U - fV + gH\frac{\partial \zeta}{\partial x} + \kappa U = F_U \tag{5.5.11}$$

$$i\omega V + fU + gH\frac{\partial \zeta}{\partial y} + \kappa V = F_V \tag{5.5.12}$$

$$\left(\frac{\partial U}{\partial x} + \frac{\partial V}{\partial y}\right) + i\omega\zeta = 0 \tag{5.5.13}$$

where ω is frequency of a tidal constituent, U and V are x and y components of current integrated from sea surface to bottom, respectively, f is Coriolis parameter, g is acceleration of gravity, H is depth, ζ is the anomaly from mean sea level, κ is dissipation coefficient of bottom friction, F is tide-generating force.

We use Ensemble Transform Kalman Filter (ETKF) (Bishop *et al.* 2001) to assimilate harmonic constants at tide stations. Since the model result has errors due to the resolution and accuracy of bathymetry data and lateral boundary conditions, perturbations are added to bathymetry and boundary condition in order to create an ensemble. We have prepared 120 ensemble members which are combinations of 30 different data sets of bathymetry including random errors and boundary condition generated by blending the results of tidal models and 4 bottom friction data. The tidal models used are NAO.99Jb (Matsumoto *et al.* 2000), FES2004 (Lyard *et al.* 2006), GOT00.2 (an update to Ray (1999)), and TPXO (Egbert and Erofeeva 2002). Minor 19 constituents are estimated from major constituents of similar frequency using the response method (Munk and Cartwright 1966).

5.5.3.4 Long-period Tides

The first guess of annual constituents (S_a) is derived from the result of harmonic analysis of reanalyzed sea level height from MOVE/MRI.COM (see Section 5.3 and Usui *et al.* (2006)) corrected with sea surface pressure

from Japanese 25-year Reanalysis (JRA-25) and JMA Climate Data Assimilation System (JCDAS) (see Section 2.10 and Onogi *et al.* (2007)) assuming hydrostatic balance. This is modified using harmonic constants at tide stations by optimal interpolation (OI) method.

5.5.3.5 Verification

To verify the astronomical tides analyzed by the described method, we compared them with those from harmonic constants at tide stations. Figure 5.5.10 shows the distribution of root mean square error (RMSE) of the analysis compared with those from harmonic constants of tide stations. At most of the stations, RMSE is less than 3cm, while at some stations especially in bays and inland sea, RMSE is relatively large.

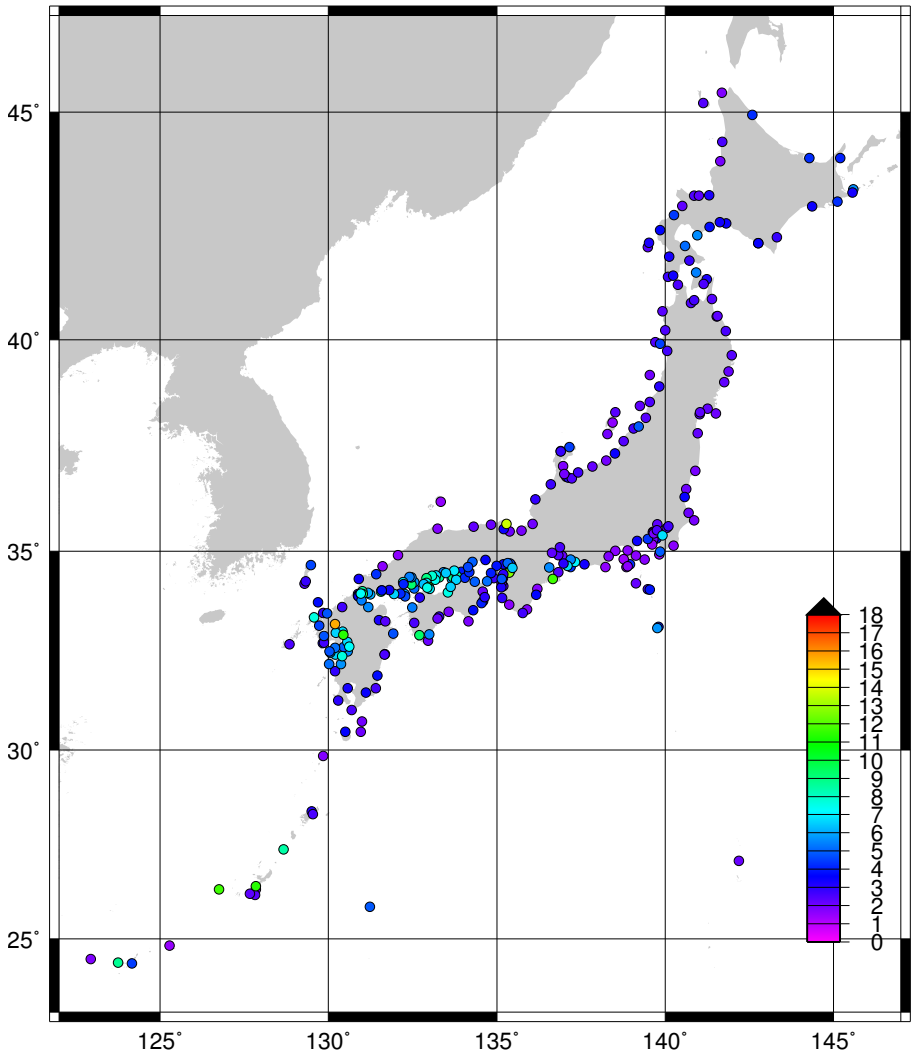

Figure 5.5.10: Distribution of RMSE of astronomical tide analysis. The unit is cm.

5.6 Sea Ice Model

5.6.1 Introduction

The Japan Meteorological Agency (JMA) has operated a numerical sea ice model since December 1990 to support sea ice forecasting for the southern part of the Sea of Okhotsk in the winter season. The sea ice model based on dynamics and thermodynamics forecasts distribution and concentration of sea ice for the next 7 days.

Outputs of the model have been operationally disseminated twice a week for the duration of sea ice around Hokkaido, the northern island of Japan, via internet[5] and through JMH broadcast system.

5.6.2 Model Structure

5.6.2.1 Forecast Area

Figure 5.6.1 shows the forecast area with 71×71 square grids with intervals of 12.5km. The model calculates 4 physical elements (volume, concentration, velocity and thickness (=volume/concentration)) of sea ice at each grid by using initial data of sea ice concentration and sea surface temperature (SST), meteorological forecast data and statistics of ocean current.

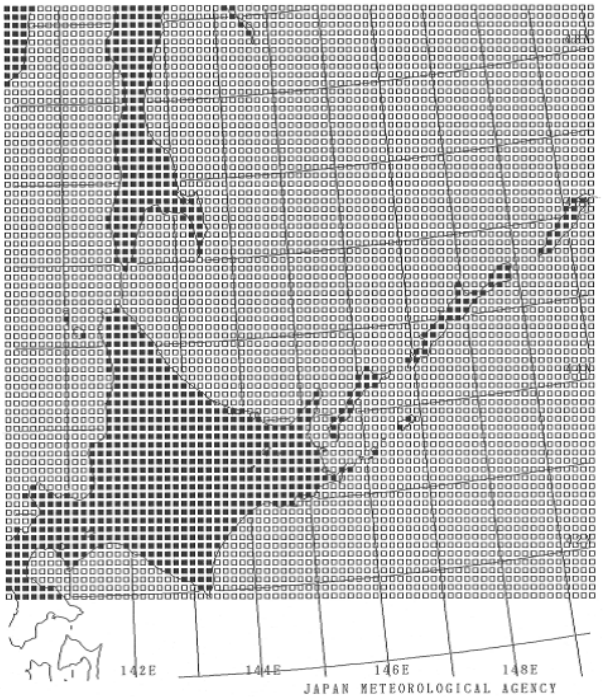

Figure 5.6.1: Forecast area of the sea ice model. ■: a land grid □: a sea grid

5.6.2.2 Calculation of Sea Ice Condition

The volume (M_i) and the concentration (A_i) of sea ice at each grid are governed by the following equations:

$$\frac{\partial M_i}{\partial t} = -\mathrm{div}(M_i V_i) + P_M$$

[5] `http://www.data.kishou.go.jp/kaiyou/db/seaice/forecast/nsif.html` (in Japanese) and `http://www.jma.go.jp/jmh/jmhmenu.html` (in Japanese)

$$\frac{\partial A_i}{\partial t} = -\mathrm{div}(A_i V_i) + P_A + D_A \tag{5.6.1}$$

where V_i is the sea ice velocity, which is determined in the dynamical process described in Subsection 5.6.2.3. P_M and P_A denote the change of the volume and the concentration, respectively, due to the growth or the melting of sea ice and snowfall. They are determined in the thermodynamic process described in Subsection 5.6.2.4. D_A is a term related to the development of hummock due to the convergence of sea ice. D_A is given by calculating the convergence of V_i : (Udin and Ullerstig 1976)

$$D_A = \begin{cases} \mathrm{div}(A_i V_i) & A_i = 1 \quad \text{and} \quad \mathrm{div}(V_i) < 0 \\ 0 & 0 < A_i < 1 \quad \text{or} \quad \mathrm{div}(V_i) \geq 0. \end{cases} \tag{5.6.2}$$

5.6.2.3 Dynamical Processes

A momentum equation of sea ice is described as follows: (Hibler 1979)

$$\rho_i H_i \frac{\partial V_i}{\partial t} = \tau_a(V_a) + \tau_w(V_w, V_i) + C(V_i) + G(V_w) + F_i \tag{5.6.3}$$

τ_a : wind stress,
τ_w : water stress,
C : Coriolis force,
G : pressure gradient force due to tilting sea surface,
F_i : internal ice stress.

Here ρ_i and H_i ($=M_i / A_i$) are sea ice density and thickness, respectively. V_a, V_w, and V_i denote the velocity of wind, ocean current and sea ice, respectively. Due to the fact that the left-hand side term of Eq. (5.6.3) is smaller than the other terms by more than one order of magnitude, V_i can be derived approximately on the assumption that the terms on the right-hand side terms of Eq. (5.6.3) are in balance. V_a is given by Global Spectral Model (GSM, see Section 3.2) and V_w is given by climatology described in Subsection 5.6.3.3. We simplified Hibler's viscous-platic method to calculate F_i because F_i is such a quite complex term that we used a lot of computational resources. The alternate method is that a provisional sea ice velocity calculated by the assumption that the first 4 terms of Eq. (5.6.3) are balanced is modified by the non-slip condition at the coastal square grids.

5.6.2.4 Thermodynamic Processes

The thermodynamic processes in the model effect the growth or the melting of sea ice by heat exchange among atmosphere, ocean and sea ice. In sea ice area, heat exchange between atmosphere and sea ice causes the change of sea ice thickness. A heat balance equation on the sea ice surface is as follows (Semtner 1976):

$$(1 - Al)R_s \downarrow + R_a \downarrow + SH(T_i) \downarrow + LH(T_i) \downarrow - FL(T_i, H_i) \downarrow - R_i(T_i) \uparrow = 0 \tag{5.6.4}$$

R_s : solar radiation,
Al : albedo of sea ice or snowfall,
R_a : atmospheric radiation,
SH : sensitive heat flux,
LH : latent heat flux,
FL : vertical heat flux in sea ice,
R_i : radiation emitted from sea ice,
T_i : surface temperature of sea ice.

R_s and R_a are given by GSM. T_i can be calculated from Eq. (5.6.4). If $T_i < -1.8$°C, sea ice gains the thickness whose increment is estimated from FL. If $T_i > 0$°C, sea ice loses the thickness whose negative increment is estimated from the sum of all the terms on the left-hand side of Eq. (5.6.4) after T_i is set to 0°C. If -1.8°C $\leq T_i \leq 0$°C, sea ice remains unchanged.

In open water area, heat exchange between atmosphere and ocean causes change of sea water temperature that affects melting sea ice. The ocean in the model consists of a thin surface layer and a mixed layer. The amount of heat exchange between the ocean and the atmosphere at each grid is described as follows:

$$Q_w \downarrow = (1 - Al_w)R_s \downarrow + R_a \downarrow + SH(T_s) \downarrow + LH(T_s) \downarrow - R_w(T_s) \uparrow \tag{5.6.5}$$

Here R_w denotes the radiation emitted from sea surface and Al_w is the albedo of sea water. T_s is the sea water temperature of the surface layer. We assume that the heat exchange between the sea surface layer and the mixed layer is calculated as follows:

$$T_s = \frac{(T_s - T_f)D_s + (T_m - T_f)D_m}{D_s + D_m} + T_f \tag{5.6.6}$$

Here D_s and D_m denote the depth of the surface layer and the mixed layer, respectively, and are fixed at each sea grid. T_m is the sea water temperature of the mixed layer, and T_f is the freezing point (-1.8°C) of sea water. Here, the change of sea water temperatures is calculated on the two assumptions that direct heat exchange between sea ice and sea water occurs only through the surface layer and that the heat exchange between sea ice and the surface layer occurs to drive T_s to the melting point (0°C).

5.6.3 Data Used in the Model

5.6.3.1 Initial Data of Sea Ice and Sea Surface Temperature

Initial fields of sea ice and sea surface temperature are derived from data as follows: Initial fields of sea ice concentration is subjectively estimated on the basis of data from satellites (mainly MTSAT and NOAA), aircraft, ships and coastal observations; An initial field of sea ice thickness is derived from the previous forecast; Daily SST analysis data in the seas around Japan given by MGDSST, which is described in Subsection 5.2.1, are used for an initial field of SST.

5.6.3.2 Meteorological Data

Air pressure, air temperature, wind, dew point, solar radiation, atmospheric radiation and precipitation on the sea surface at each grid are given by the interpolation of the predictions by the atmospheric numerical model (GSM).

5.6.3.3 Ocean Current Data

The distribution of the ocean currents used in the model is obtained from Japan Maritime Safety Agency (1983) and shown in Figure 5.6.2. It is fixed throughout the winter season.

5.6.4 Example of the Results of the Numerical Sea Ice Model

An example of the results of the 7-day forecast is shown in Figure 5.6.3. In this example the model forecasts that sea ice will move southward and be on the coast of the Hokkaido Island facing the Sea of Okhotsk.

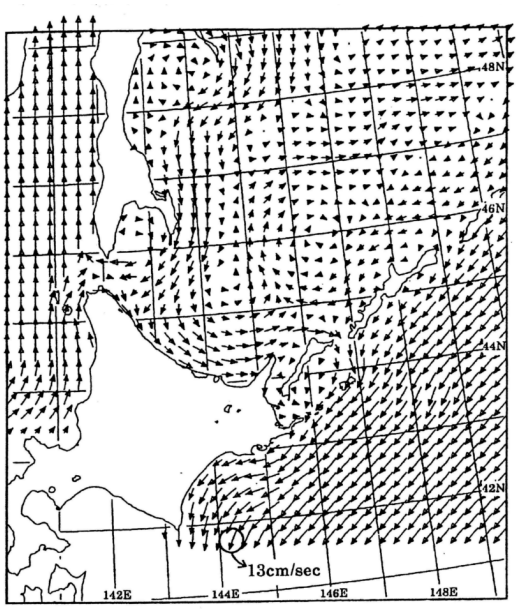

Figure 5.6.2: The ocean currents used in the model.

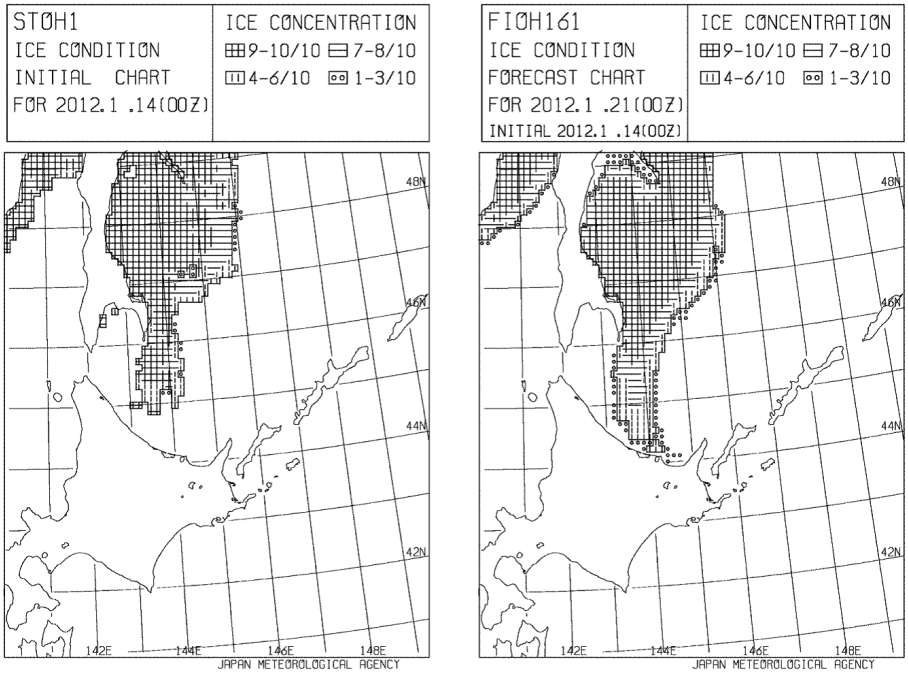

Figure 5.6.3: An example of the results of the model.

5.7 Oil Spill Prediction Model

5.7.1 Introduction

In 1990s, large-scale oil spill incidents frequently occurred in the world. Around Japan, a wrecked Russian tanker "Nakhodka" brought about a severe oil spill incidents in the Sea of Japan in January 1997, which led to heavy damage to the environment along the western coastline of the Japan. After the incident, countermeasures against large-scale oil spill events were considered in the Japanese Government, and JMA developed an Oil Spill Prediction Model, and the model has been put into operational mode since October 1999.

The model predicts large scale behavior of spilled oil in offshore seas where tidal current is negligible. Getting accident information from the Japan Coast Guard, JMA operates the Oil Spill Prediction Model to get up to 192 hours forecast, and results are transferred to the staff who is responsible for emergency response operations.

The prediction model is applicable to the entire western North Pacific. The domain of calculation is selected from prepared seven settings from $0.8^\circ \times 0.8^\circ$ to $12^\circ \times 12^\circ$ in latitude and longitude, by considering of the incident condition.

5.7.2 Basic Equation

An oil spill prediction model is generally described in the following equation including the terms of advection and diffusion,

$$\frac{dC}{dt} = \frac{\partial C}{\partial t} + \mathbf{V} \cdot \nabla C = \nabla \cdot (K \nabla C) + S \tag{5.7.1}$$

where C is the concentration of the pollutant, t is time, $\mathbf{V}$ the advection velocity, K the turbulent diffusion coefficient, and S (called the source term) represents processes to change the total amount of the spilled oil through the change of oil properties.

To solve the equation (5.7.1) with a computer, there are two common ways: one is to calculate C values directly by the finite difference method; the other is to simulate the behaviors of many 'particles' which are supposed to be the components of oil. The Oil Spill Prediction Model in JMA uses the latter method. The spilled oil is expressed by many particles $C_n (n = 1, 2, \cdots)$ as,

$$C_n \{\mathbf{x}(t + \delta t), s(t + \delta t); t + \delta t\} = \Phi[C_n (\mathbf{x}(t), s(t); t)] \tag{5.7.2}$$

where $\mathbf{x} = (x, y, z)$ indicates the position of each particle, s is the chemical status of oil. Φ is a general function which describes the oil property change in time.

In the advection term, effects of the surface wind, the ocean wave, and the ocean current could be major processes to be taken into account. Ekman drift current is generated by the sea surface wind, which is well-known as "3% rule". In the JMA model, the surface flows are determined as 2.5% of the wind speed with an angle of 15° clockwise with respect to the wind direction. The Stokes drift is a forwarded movement of particles at the sea surface to the wave direction by the wave motion back and forth in each wave cycle. This effect becomes important if high waves exist and the effect is independent of wind when swell is predominant. Therefore, Stokes drift is included explicitly and calculated from the wave condition predicted by JMA wave models. Ocean currents are provided by the JMA Ocean Data Assimilation System for the Western North Pacific (MOVE-WNP).

The three dimensional diffusion of oil is basically calculated by the sheer diffusion treatment by Elliott (1986). The surface flow is supposed to have a logarithmic profile in vertical, and spilled oil is assumed to be carried by horizontal speed at each water level. The sheer mechanism considers the vertical diffusion too. The spilled oil is divided into many oil droplets, which get the buoyancy according to their size. By considering the buoyancy and the present depth of oil drop, the oil motion in vertical, whether it remains in surface or not, is determined.

In addition to the above sheer diffusion process, there may be isotropic diffusion generated by small scale eddies and so on. This effect is estimated by the constant diffusion coefficient $K_h = 95.0 m^2/s$. In the condition

Table 5.7.1: Specification of the oil spill prediction model

Applicable area		10°S – 65°N, 120°E – 180°E
Domain of calculation		7 options ($0.8^\circ \times 0.8^\circ - 12^\circ \times 12^\circ$)
Grid spacing		7 options (2 – 30km), according to the domain of calculation
Number of grids		41×41
Prediction period		192 hours
Physical and chemical process	Advection	Ekman drift (estimated from wind field of Global Spectrum Model) Stokes drift (estimated from wave field of Global/Coastal Wave Models) Ocean current (MOVE/MRI.COM-NWP)
	Diffusion	Elliott (1986) etc.
	Evaporation	Fingas (1997)
	Emulsification	Reed (1989)

of strong winds or high ocean waves, diffusion may be enlarged. Therefore, these diffusions are parameterized with additional diffusion coefficients:

$$\begin{cases} waves : K_{wv} = 500.0 H_w^2 / T_w \\ winds : K_{wnd} = 5.0 W^5 / g \end{cases} \tag{5.7.3}$$

where H_w and T_w are wave height and period, W is wind speed, and g is the gravitational acceleration.

The additional diffusion of oil parcels are estimated by the total value of the diffusion coefficients (K_h, K_{wv}, and K_{wnd}). The concrete values are calculated by the random walk method and this diffusion is supposed to be horizontal.

Since the behavior of spilled oil is quite complicated, it is difficult to consider all of the chemical processes. We only consider a few of major processes, that is, evaporation and emulsification. The evaporation is estimated by the Fingas's empirical formulae (Fingas 1997). According to Fingas (1997), the evaporation rate $E_v(\%)$ of most oils can be expressed by the form of either the logarithmic or root profile in time.

$$E_v = \begin{cases} (a + b \cdot T) \ln t \\ (a + b \cdot T) \sqrt{t} \end{cases} \tag{5.7.4}$$

The constant coefficients a and b were determined by experiments and are listed in the oil data catalogue by Environment Canada. T stands for the temperature of oil which is supposed to have the same value of the Sea Surface temperature (SST), t is the elapsed time (in minute) after the spill.

The emulsification is calculated by the formula of Reed (1989), which estimates the water content F_{wc} by

$$\frac{dF_{wc}}{dt} = 2.0 \times 10^{-6} (W + 1)^2 \cdot \left(1 - \frac{F_{wc}}{C_3}\right) \tag{5.7.5}$$

where $W(m/s)$ is wind speed. C_3 is a constant parameter for the upper limit of water content, which differs among the oil types. The density of oil is also calculated with the water content, which can change the behaviour of oil.

Specifications of the Oil Spill Prediction Model and process methods used in the model are summarized in Table 5.7.1

5.7.3 Products

The model is to be operated in the case of a large-scale oil spill in the offshore deep water seas where tidal currents in short time can be negligible. The result of oil spill prediction is provided to the Japanese Government and/or the Japan Coast Guard with the other various marine meteorological charts. An example of the prediction is shown in Figure 5.7.1.

5.7.4 Development Plan

The current model is going to be replaced by a new version written in fortran90. In the current version, the model domain and resolution must be chosen from seven options, because of the restriction of setting in FORTRAN77. On the other hand, dynamic array allocation is available in fortran90. Therefore, in the new version, the model domain and grid resolution can be set freely, so as to be suitable for the incident condition.

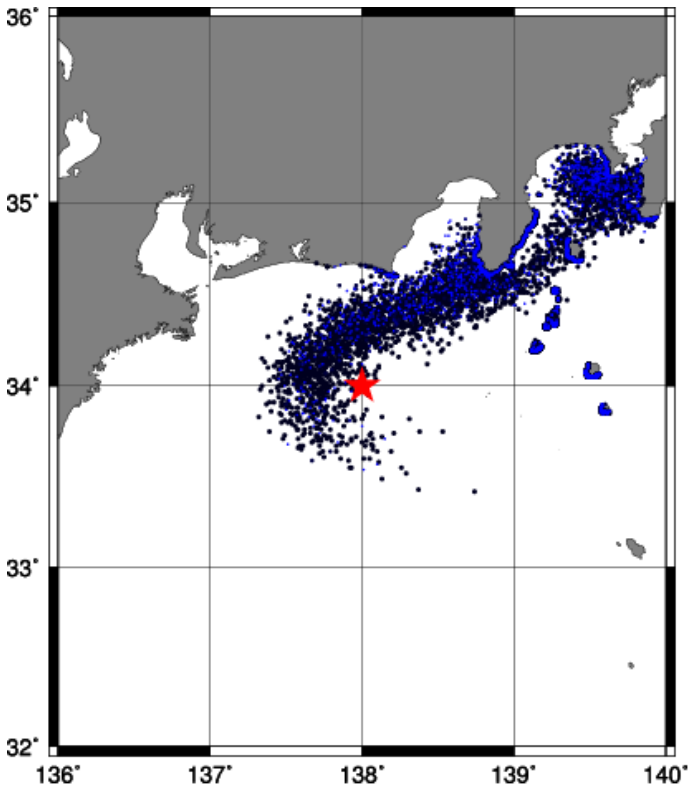

Figure 5.7.1: An example of a test simulation case in the sea south of Japan. The star shows the locations of the accident. The area and amount of the spilled oil is indicated by dot distribution.